DEPARTMENT OF AEROSPACE ENGINEERING
COLLEGE OF ENGINEERING & TECHNOLOGY
OLD DOMINION UNIVERSITY
NORFOLK, VIRGINIA 23529

PRELIMINARY EDDY CURRENT MODELLING FOR THE LARGE ANGLE MAGNETIC SUSPENSION TEST FIXTURE

By

Colin Britcher, Principal Investigator

Progress Report
For the period May 1, 1993 to October 31, 1993

Prepared for
National Aeronautics and Space Administration
Langley Research Center
Hampton, Virginia 23681

Under
Research Grant NAG-1-1056
Nelson J. Groom Technical Monitor
Guidance and Control Division

January 1994

DEPARTMENT OF AEROSPACE ENGINEERING
COLLEGE OF ENGINEERING & TECHNOLOGY
OLD DOMINION UNIVERSITY
NORFOLK, VIRGINIA 23529

PRELIMINARY EDDY CURRENT MODELLING FOR THE LARGE ANGLE MAGNETIC SUSPENSION TEST FIXTURE

By

Colin Britcher, Principal Investigator

Progress Report
For the period May 1, 1993 to October 31, 1993

Prepared for
National Aeronautics and Space Administration
Langley Research Center
Hampton, Virginia 23681

Under
Research Grant NAG-1-1056
Nelson J. Groom Technical Monitor
Guidance and Control Division

Submitted by the
Old Dominion University Research Foundation
P.O. Box 6369
Norfolk, Virginia 23508

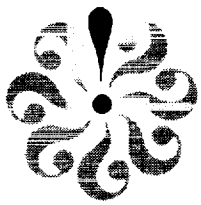

January 1994

PRELIMINARY EDDY CURRENT MODELLING
for the
LARGE ANGLE MAGNETIC SUSPENSION TEST FIXTURE

Colin P. Britcher, Lucas E. Foster
Department of Aerospace Engineering
Old Dominion University
Norfolk, VA

SUMMARY

This report presents some recent developments in the mathematical modelling of the Large Angle Magnetic Suspension Test Fixture (LAMSTF) at NASA Langley Research Center. It is shown that these effects are significant, but may be amenable to analysis, modelling and measurement. A theoretical framework is presented, together with a comparison of computed and experimental data.

INTRODUCTION

In order to explore and develop technology required for the magnetic suspension of objects over large ranges of orientation, a small-scale laboratory development system, the Large Angle Magnetic Suspension Test Fixture (LAMSTF) has been constructed at NASA Langley Research Center. Possible applications for magnetic suspension systems of this general class include space payload pointing and manipulation, microgravity vibration isolation and wind tunnel model suspension [1]. An important objective of this particular project is to investigate the dynamic modelling of large-gap magnetic suspension systems, so that future systems can be designed with higher confidence levels.

EDDY CURRENT EFFECTS IN LAMSTF

Introduction

Whenever a time-varying magnetic flux penetrates a conducting medium, eddy-currents will be generated. In the case of LAMSTF, the principal time variation is due

to the necessary control forces and torques being generated by fluctuating electromagnet currents, since the system is open-loop unstable. In the original design, eddy-current circuits were deliberately introduced in three main areas, as illustrated in Figure 1 :

1) Position sensor structure, 2) Electromagnet cores, 3) Aluminum baseplate

This was done so that it would be necessary to measure, analyse and model the eddy current effects, rather than attempting to avoid their influence, as is the usual practice. The fact that stable suspension was initially achieved rather easily [2] was taken to indicate that the eddy current effects were not very significant. However, a consistent discrepancy has been found in the dynamic behaviour in the "pitch" degree-of-freedom [3,4]. In consequence, an analysis and modelling effort has now been undertaken.

Eddy Current Modelling

A simplified analysis can be employed to assess the effects of eddy currents in LAMSTF. The two key assumptions are some a priori knowledge of the geometry of the eddy current circuit and that the circuit geometry be independent of frequency. The first assumption might require that the eddy currents be constrained to flow around well-defined paths, such as the position sensor structure, rather than through large plates or shells of conducting material. Alternatively, the circuit geometry must be relatively simple and predictable. The second assumption requires that the "skin depth" be much greater than the local material thickness. The skin depth is given by the following formula [5] :

$$d = \sqrt{\left(\frac{2}{\mu_0 \mu_r \sigma \omega}\right)} \quad \text{or} \quad \sqrt{\left(\frac{2\rho}{\mu_0 \mu_r \omega}\right)} \qquad \text{- (1)}$$

- where d = Skin depth, μ = Permeability, $\rho = 1/\sigma$ = Resistivity, ω = angular frequency. In the case of LAMSTF, the natural frequencies of the suspended element are rather low, of the order of 10Hz or less. For an aluminum conductor, the skin depth at 10Hz would be around 28mm, much greater than the typical material thickness in LAMSTF. The only exceptions are the iron electromagnet cores, although it is found later that their influence is confined to higher frequencies.

If both of the above assumptions are satisfied, the resulting model corresponds to that commonly described in literature as the Single Time Constant Model. The derivation now resembles the analysis of a transformer with a shorted secondary, as

illustrated in Figure 2 :

$$V = IR + L\frac{dI}{dt} + L_{m_1}\frac{dI_{e_1}}{dt} + L_{m_2}\frac{dI_{e_2}}{dt} + \cdots \qquad - (2)$$

$$0 = I_{e_1}R_{e_1} + L_{e_1}\frac{dI_{e_1}}{dt} + L_{m_1}\frac{dI}{dt} \qquad - (3)$$

- where R_{e_n}, L_{e_n} are the resistance and inductance of the n'th eddy current circuit and L_{m_n} is the mutual inductance between the primary (the electromagnet coil) and the eddy current circuit. Note that mutual inductances between multiple eddy current circuits are neglected. The terminal characteristics of the primary (driven coil) can be found by combining these two equations :

$$\frac{I}{V} = \left(\frac{1}{(R + Ls) - \dfrac{(L_{m_1}s)^2}{R_{e_1} + L_{e_1}s} - \cdots} \right) \qquad - (4)$$

One special case is of interest here. Suppose that :

$$L = \alpha L_{e_1} \ (\ 0 \leq \alpha \leq \infty \ ) \quad \text{and} \quad L_{m_1} = \beta \sqrt{(L\ L_{e_1})} \quad (\ 0 \leq \beta \leq 1) \qquad - (5)$$

then :

$$\frac{I}{V} = \left(\frac{1}{(R + Ls) - \dfrac{\beta^2 \alpha\ (L_{e_1}s)^2}{R_{e_1} + L_{e_1}s} - \cdots} \right) \qquad - (6a)$$

but if $R_{e_1} \rightarrow 0$ or $s \rightarrow \infty$:

$$\frac{I}{V} = \left(\frac{1}{R + Ls\ (1-\beta^2)} \right) \qquad - (6b)$$

This indicates that a non-dissipative (reactive) secondary effectively "turns off" part of the primary inductor. Continuing, the field components generated (at the suspended object) can be expressed as :

$$B_j = K_j I + K_{e_1} I_{e_1} + \cdots = K_j I \left(1 - \frac{K_{e_1} L_{m_1} s}{K_j (R_{e_1} + L_{e_1} s)} - \cdots \right) \qquad - (7)$$

- where K_j, K_{e_n} are constants representing the field generated at the suspension location by the electromagnet and the n'th eddy current respectively. Now the factor K_{e_n} will, in general, be different for each field component, that is each individual eddy current will affect each field component by a different proportion. Therefore the eddy current effects in a system involving several electromagnets and eddy current circuits should be represented as follows :

$$[B_j] = [K_j] [I] + [K_{j_e}] [I_e] \qquad - (8)$$

- where $[B_j] = (B_x \; B_y \; B_z \; B_{xx} \cdots)^T$, $[I]=(I_1 \; I_2 \cdots)^T$, $[K_j]$ is a rectangular matrix of field coefficients and $[K_{j_e}]$ is similar, though possibly of differing dimension. It is presumed that $[I_e]$ can be derived from $[I]$, following equations 2,3.

Alternatively, if the eddy current circuit has similar geometry to the primary (for example the induced current in electromagnet cores), it can be argued that the relative effect on all field and field gradient components at the suspended object will be similar. In this case, the representation can be considerably simplified by invoking a false current as shown :

$$I' = \left(1 - \frac{K_{e_1} L_{m_1} s}{K_j (R_{e_1} + L_{e_1} s)} + \cdots \right) I \,, \quad \text{where } B_j = K_j I' \qquad - (9)$$

It should be noted that the change in electromagnet terminal characteristics and the change in field at the model are two separate effects and should be modelled as such.

Determination of Parameters

The question now is, can the parameters K_{e_n}, L_{e_n}, R_{e_n} and L_{m_n} be estimated and/or measured with sufficient accuracy? First the problem of estimation is addressed.

Calculations have been carried out using the finite element computer code VF/GFUN, by Vector Fields Inc.. It should be noted that this code is magnetostatic and has no capability for direct eddy current calculations, although such codes are available (for instance ELEKTRA, by the same supplier). Instead, the code is used to

calculate flux linkages, hence inductances, using :

$$\phi_{ij} = \sum_{j=1}^{n} L_{ij} I_j \qquad \text{- (10)}$$

VF/GFUN calculates the field on a grid representing the linkage plane of the eddy current circuit. The field normal to the plane is then numerically integrated (by the OPERA pre- and post-processor) to yield the flux linkage term. Figure 3 illustrates the general arrangement. The calculation of the K_{e_n} terms is straightforward.

By way of example, a series of calculations have been made for a single LAMSTF electromagnet with a representation of one part of the position sensor assembly mounted on the same axis, as illustrated in Figure 4. The required parameters were predicted (or previously measured) to be :

$L = 0.0275$ H	$R = 0.74\ \Omega$
$L_e = 6.69 \times 10^{-7}$ H	$R_e = 2.243 \times 10^{-4}\ \Omega$
$L_m = 1.0998 \times 10^{-5}$ H	
$K_z = 3.495 \times 10^{-4}$ T	$K_{z_e} = 4.369 \times 10^{-6}$ T

Incorporating these values in equation 7, and examining the axial (z-axis) field component, gives :

$$B_z = K_z I \left(1 - \frac{6.13 \times 10^{-4}\ s}{1 + 2.983 \times 10^{-3} s} \right) \qquad \text{- (11)}$$

It is seen that the reasonant frequency of this eddy current circuit is around 53Hz, significantly higher than LAMSTF open-loop natural frequencies, but still well within the range of interest.

Experimental Verification

Actual measurements of the current to field transfer function, corresponding to equation 7, were made with an experimental set-up as described above, and later with LAMSTF. Field components were measured with a F.W. Bell Model 9903 Hall-effect gaussmeter. Electromagnet currents were measured using a current shunt. The transfer function was measured directly with a Schlumberger Model SI 1250 analyzer, with sine-sweep excitation. The results for an air-cored electromagnet with no eddy current

circuits are shown in Figure 5, and are taken to represent the probe + instrument + data acquisition system response. These results are subtracted from all subsequent measurements. Figure 6 shows the measured transfer function for B_Z, together with the predictions from equation 11. The agreement is thought to be satisfactory. The values of most parameters could be adjusted (refined) to give a better agreement, also shown in Figure 6. The matching procedure is described in the Appendix. The only significant residual discrepancies are seen to occur at higher frequencies, where the validity of the Single Time Constant Model is questionable. The adjusted form of equation 11 is :

$$B_Z = K_Z I \left(1 - \frac{7.591 \times 10^{-4}\ s}{1 + 2.934 \times 10^{-3} s} \right) \qquad \text{- (11b)}$$

More Complex Cases

If the electromagnet is mounted on the aluminum plate, a second eddy current circuit is added, when the iron core is inserted, a third. Figure 7 shows the comparison between experimental and adjusted theoretical responses with only the alloy plate added. Again, the agreement is fair, although clearly improved by the refinement of parameter estimates. Figure 8 shows the response with only the iron core added. Note that, even if refinement of parameters is undertaken, the model does not correctly predict the high frequency behaviour, particularly where the iron core is present. This is due to the iron core becoming highly dissipative at these frequencies, due to its small skin depth. Figure 9 shows the responses with the alloy plate and iron core both present, and was derived simply by adding the attenuation and phase shifts from Figures 7 and 8. Since the individual (adjusted) models in Figures 7 and 8 match quite well, the relatively poor agreement in Figure 9 is most likely due to interaction between the two eddy current circuits, not yet accounted for in the theoretical model. It is clear that further elaboration of the model may be necessary.

In the case of the dissipation at high frequencies, it is thought that the introduction of an extra low-pass term in the governing equation might be a sufficient representation of the effect for modelling purposes. The general idea is illustrated in Figure 10 and equation 11c. Work is underway to evaluate whether the break frequency of the extra term can be adequately predicted from physical geometry and material characteristics.

$$B_z = K_z I \left(1 - \frac{7.591 \times 10^{-4}\, s}{1 + 2.934 \times 10^{-3} s} \right) \left(\frac{1}{1+s} \right) \qquad \text{- (11c)}$$

Terminal Characteristics

It appears to be possible to experimentally estimate certain important parameters without direct measurement of magnetic fields. Figure 11 shows a comparison of measured and computed terminal characteristics for the single LAMSTF electromagnet mentioned above. The agreement is not perfect, but sufficient to validate the approach and can, of course, be improved by adjustment of parameters.

DISCUSSION

The simple eddy current model proposed appears to be satisfactory in the case of simple eddy current circuits in conducting but non-magnetic material. Relatively straightforward computations are capable of providing reasonable estimates of important parameters, with the option of refinement based on measurements of magnetic field or electromagnet terminal characteristics. In the case of the iron electromagnet cores, or at higher frequencies, more elaborate models have been proposed (for instance [6]), but these have one potentially serious drawback. This is that the greater the elaboration in the eddy current model, the more complex the overall suspension system model becomes, and the greater the potential difficulty in manipulating this model in the process of controller synthesis using modern model-based design methods. In some applications, the simple model proposed, with parameter adjustment, may adequately describe the eddy current influence on the dynamic behaviour, hence control performance, of the system. Discrepancies at frequencies well outside (above) the controller bandwidth would be of no consequence.

CONCLUSIONS

A simple model for the effect of eddy currents in the metallic structure of LAMSTF has been proposed and validated by experiment.

Eddy currents have been shown to seriously affect field and field gradient components in the frequency range of interest, such that they must be incorporated into a system dynamic model if modern control synthesis techniques are to be fully successful.

ACKNOWLEDGEMENTS

This work was supported by NASA Langley Research Center under Grant NAG-1-1056. The Technical Monitor was Nelson J. Groom of the Spacecraft Controls Branch.

REFERENCES

1. Britcher, C.P.: Large-Gap Magnetic Suspension Systems. International Symposium on Magnetic Suspension Technology. NASA Langley Research Center, August 1991. NASA CP-3152
2. Britcher, C.P.; Ghofrani, M.; Britton, T.; Groom, N.J.: The Large-Angle Magnetic Suspension Test Fixture. International Symposium on Magnetic Suspension Technology. NASA Langley Research Center, August 1991. NASA CP-3152
3. M. Ghofrani, Approaches to Control of the Large-Angle Magnetic Suspension Test Fixture. NASA CR-191890, December 1992.
4. Groom, N.J.; Britcher, C.P.: A Description of a Laboratory Model Magnetic Suspension Test Fixture with a Large Angular Capability. 1st IEEE Conference on Control Applications, Wright-Patterson AFB, September 1992.
5. Stoll, R.L.: The Analysis of Eddy Currents. Clarendon, 1974
6. Buntenbach, R.W.: Improved Circuit Models for Inductors Wound on Dissipative Magnetic Cores. 2nd Asilomar Conference on Corcuits and Systems, 1968.

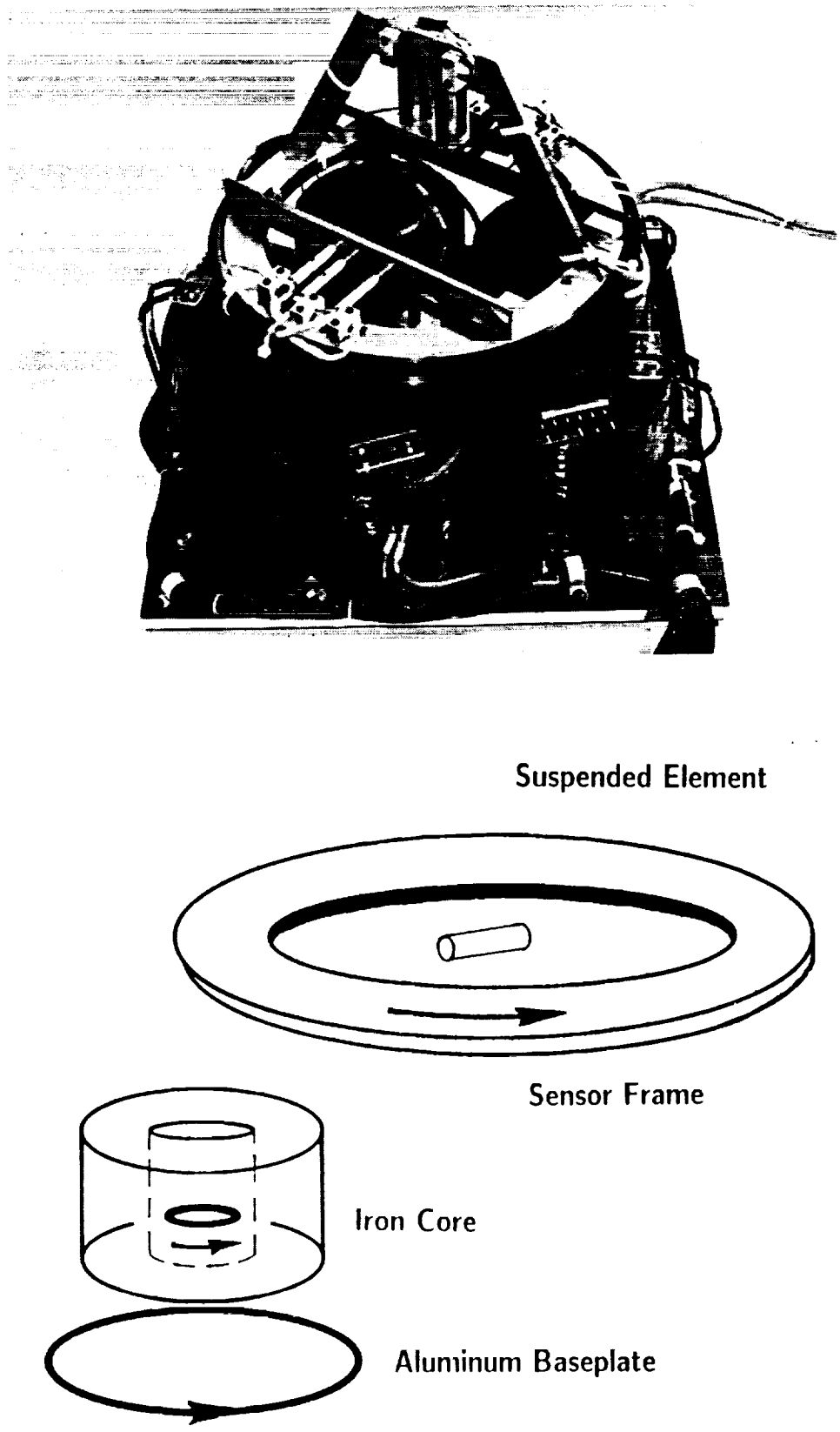

Figure 1 - Schematic Diagram of Eddy Current Circuits in LAMSTF

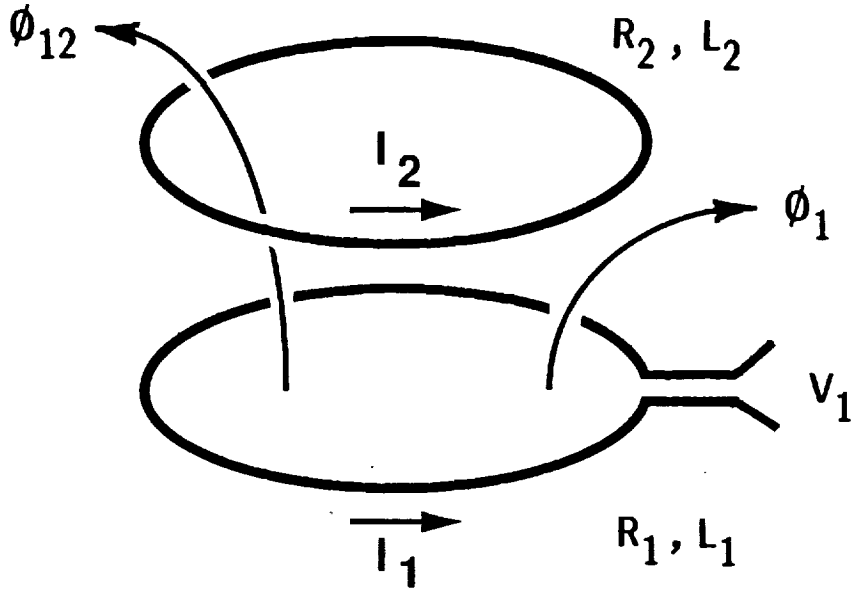

Figure 2 - Schematic of Circuit Model for Primary to Secondary Coupling

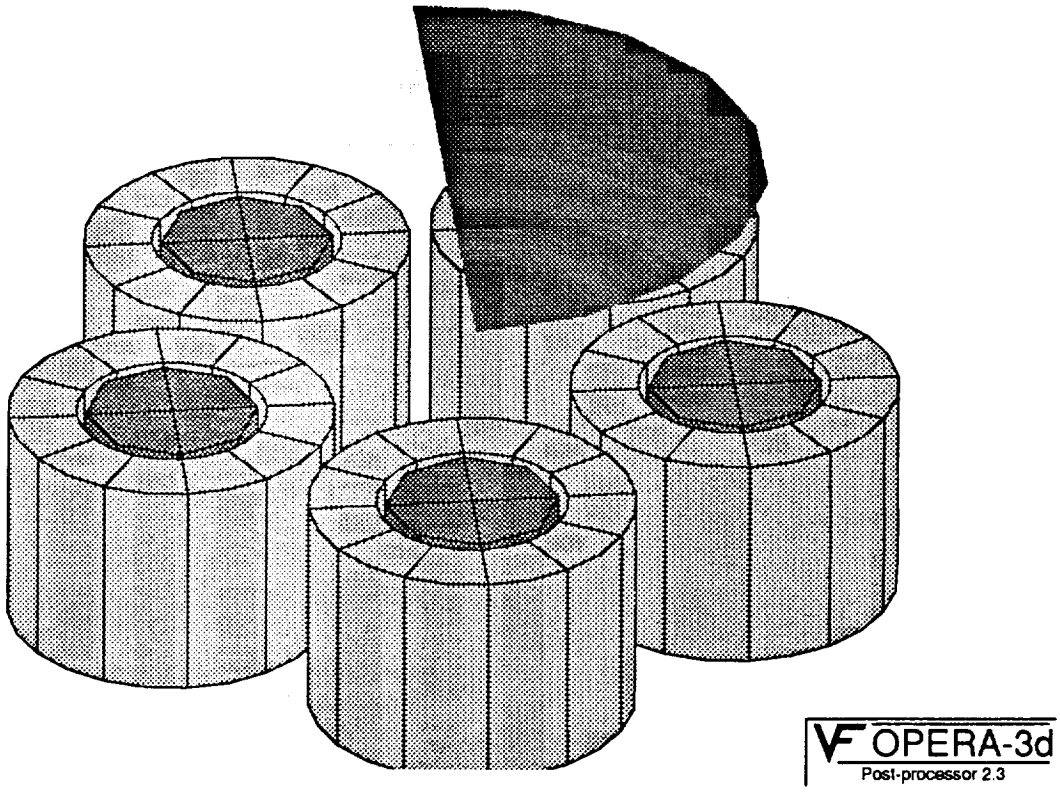

Figure 3 - Illustration of OPERA Flux Linkage Computation (B_z shown)

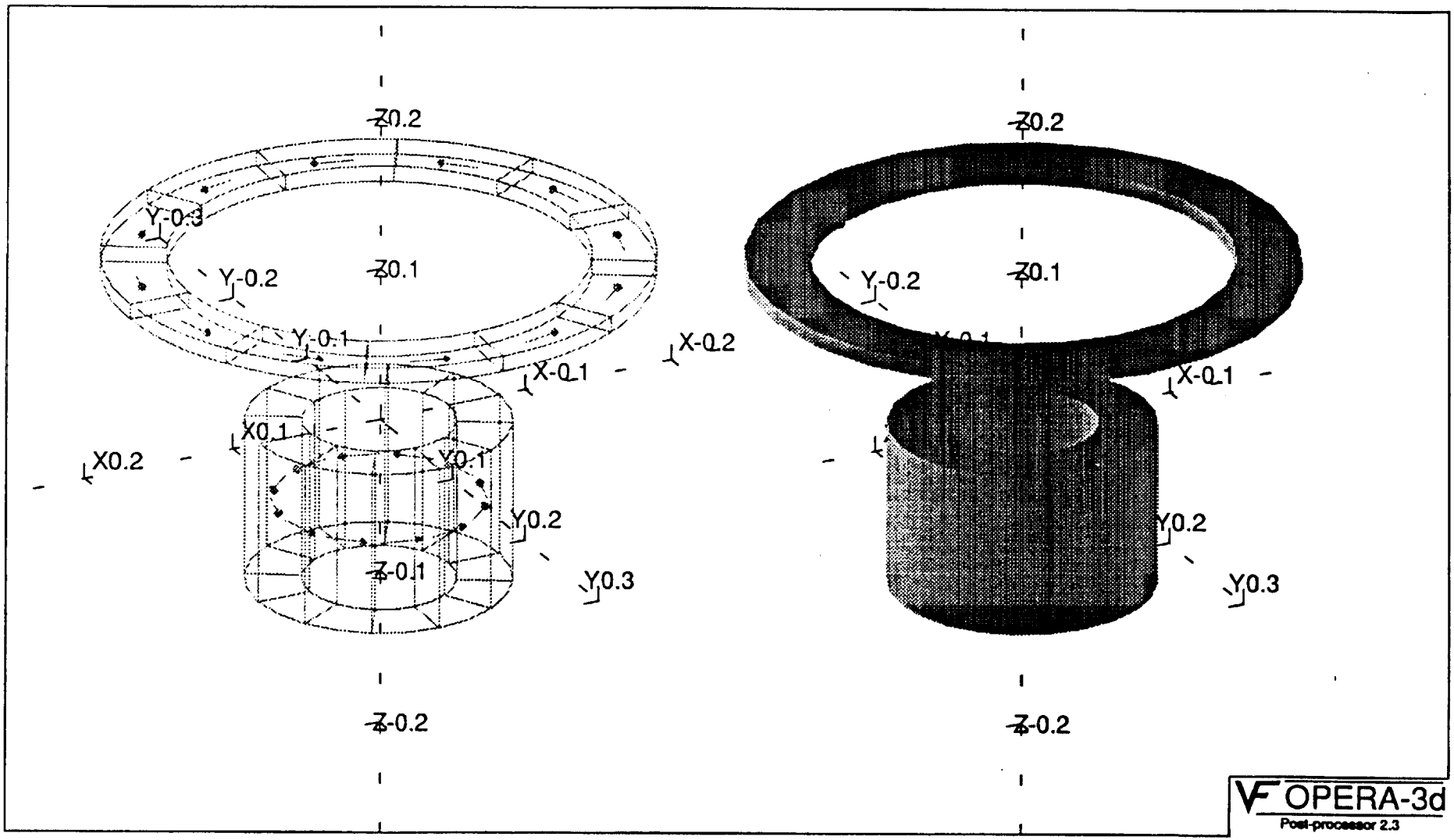

Figure 4 - Simplified Eddy Current Test Set-Up

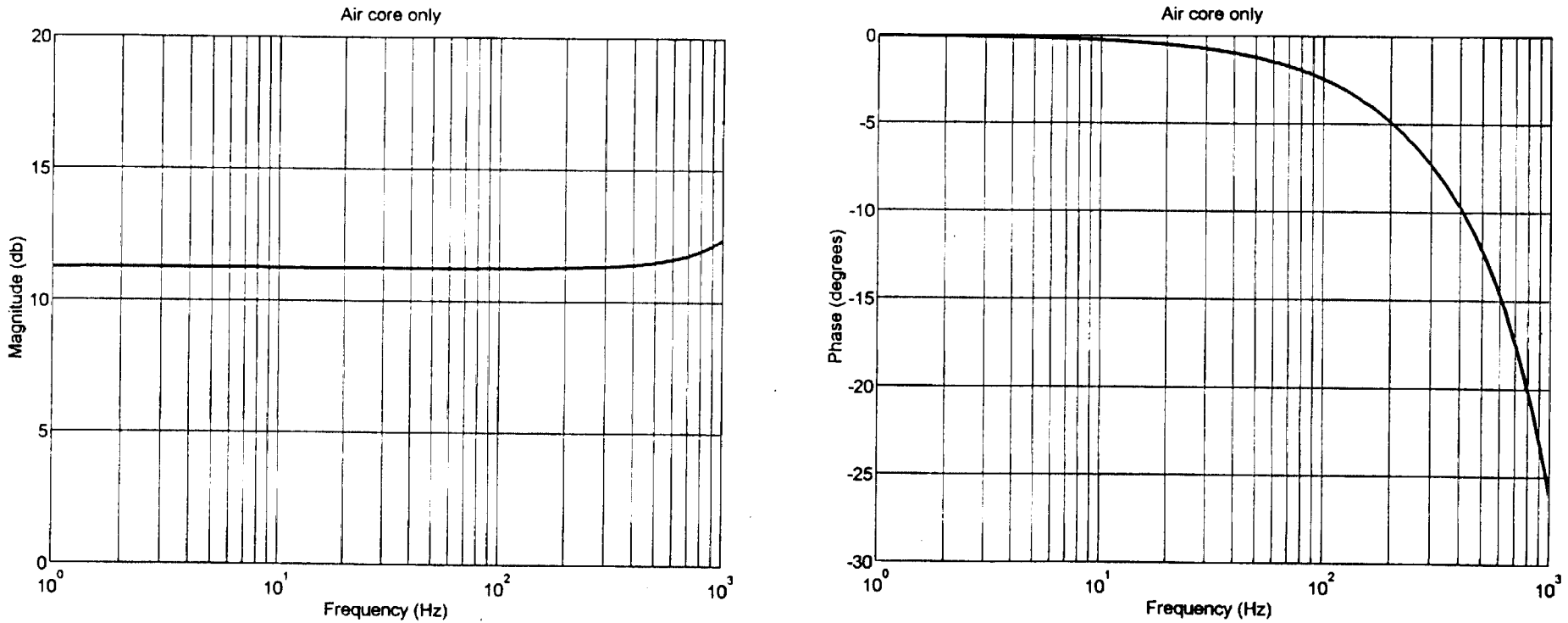

Figure 5 - Gaussmeter Probe Response

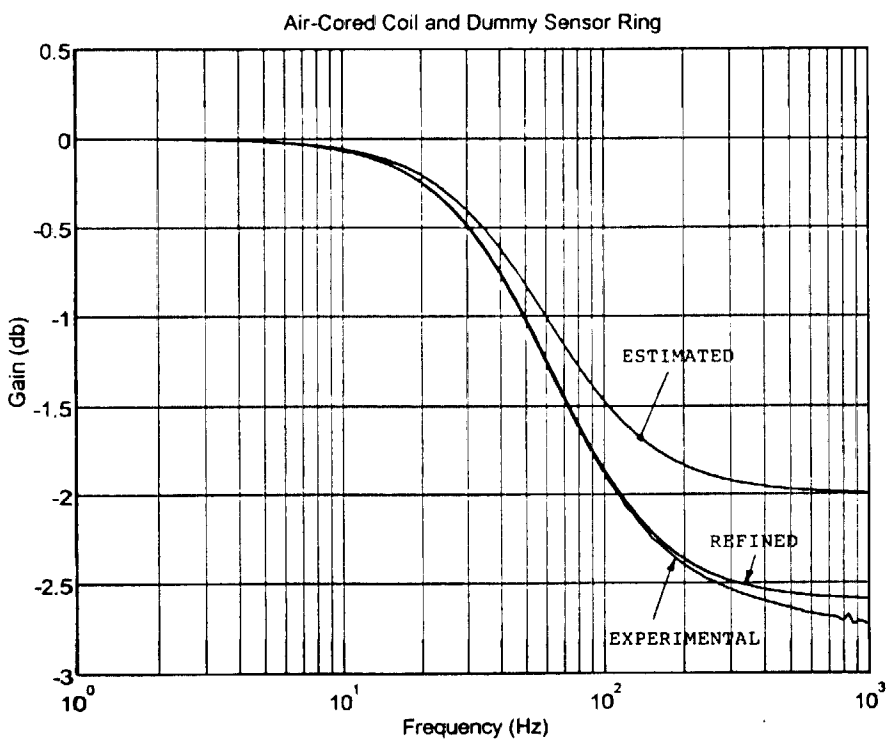

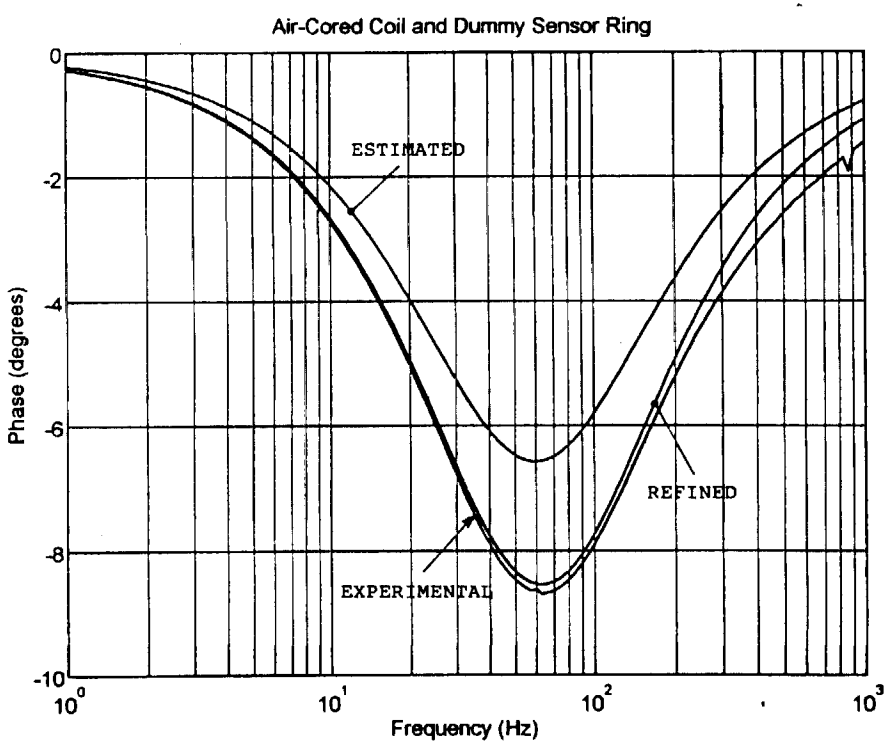

Figure 6 - Axial Field for Air-Cored Electromagnet and Dummy Sensor Ring

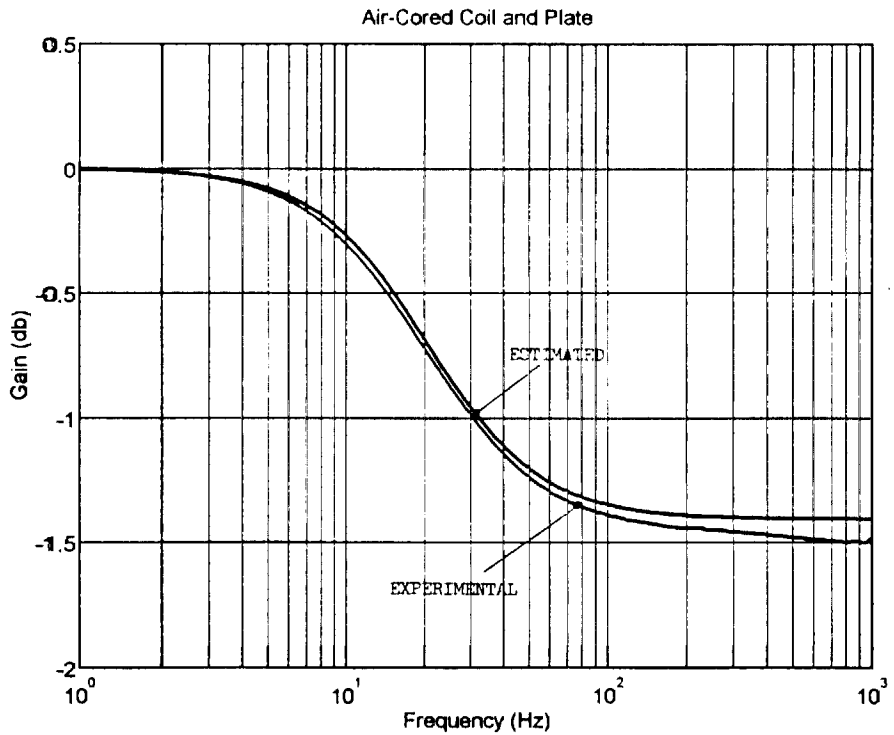

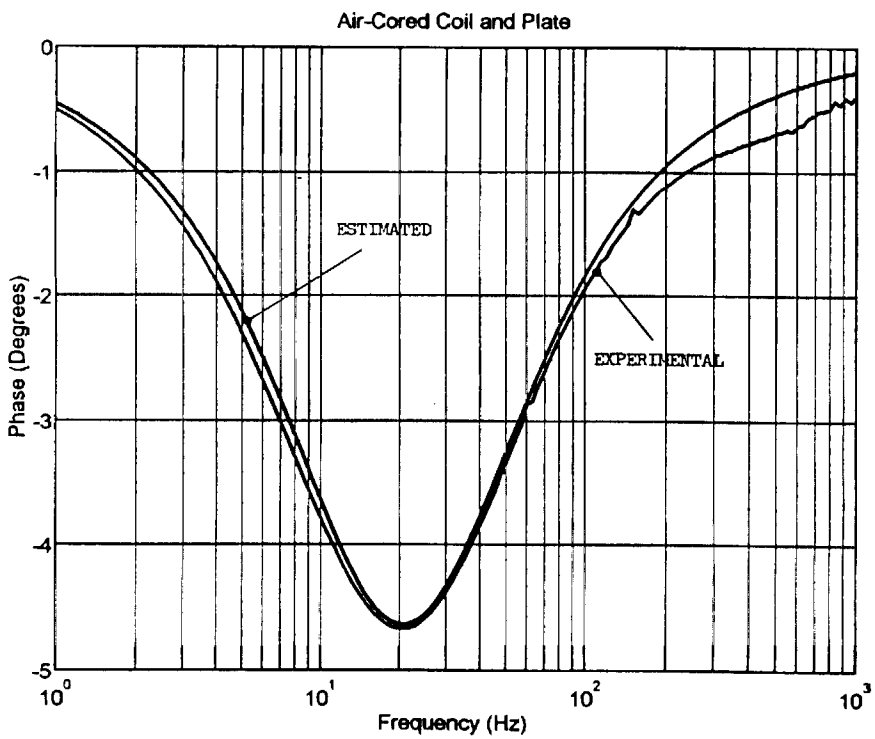

Figure 7 - Axial Field with Alloy Plate Added

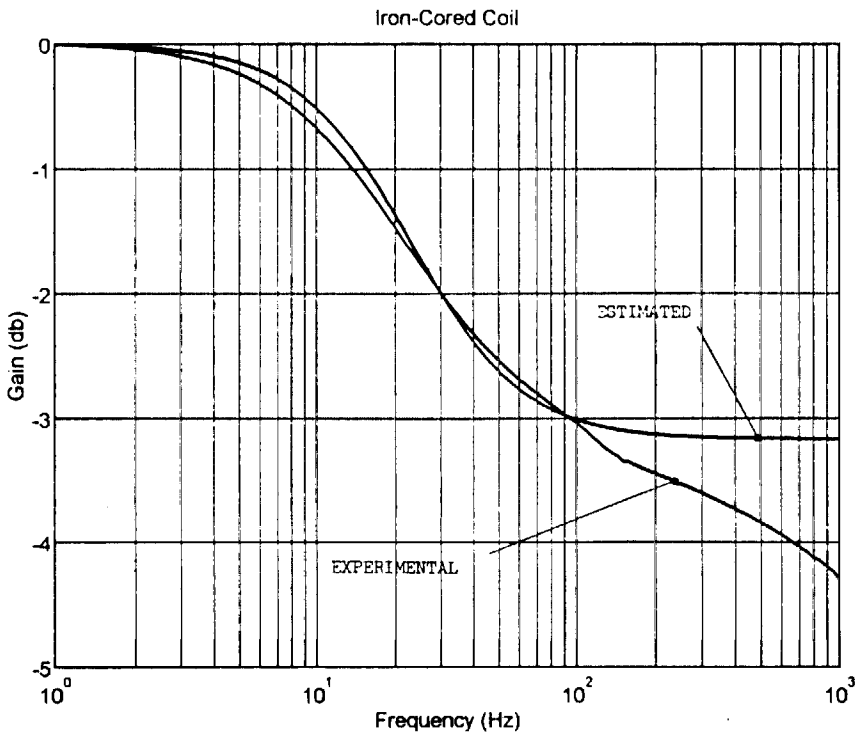

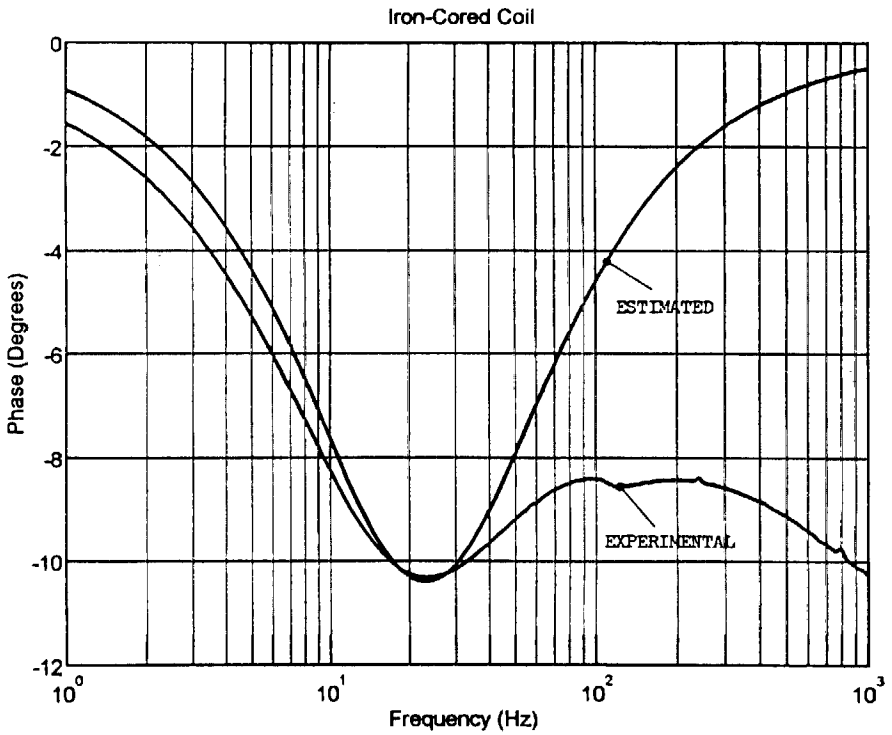

Figure 8 - Axial Field with Iron Core Added

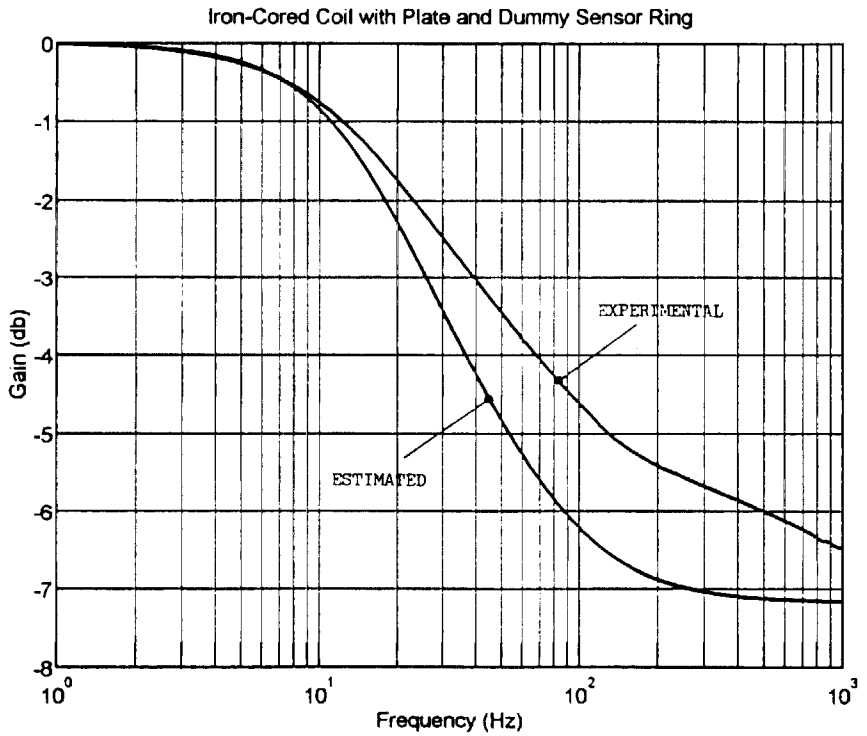

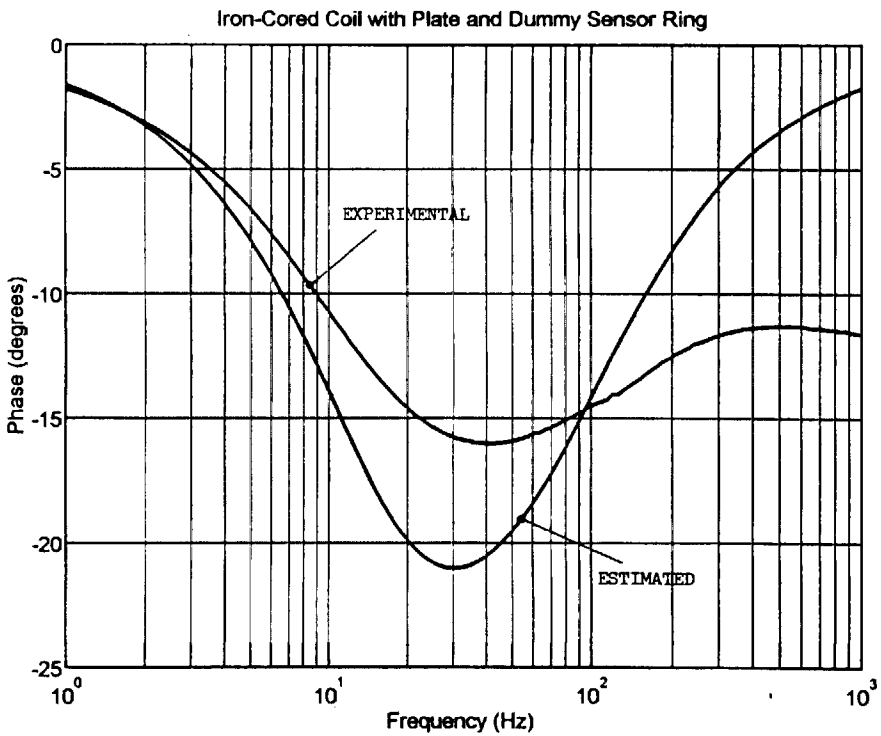

Figure 9 - Axial Field with Iron Core and Alloy Plate Added

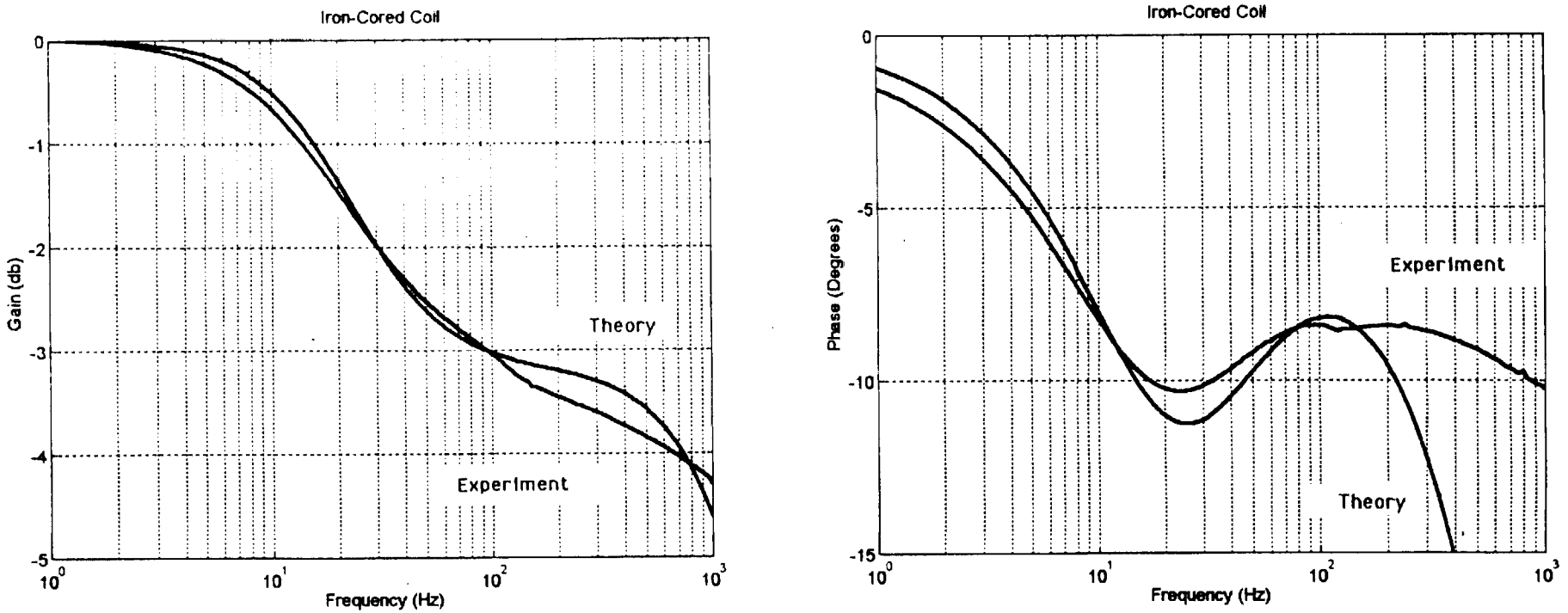

Figure 10 - Axial Field with Iron Core, showing Augmented Model

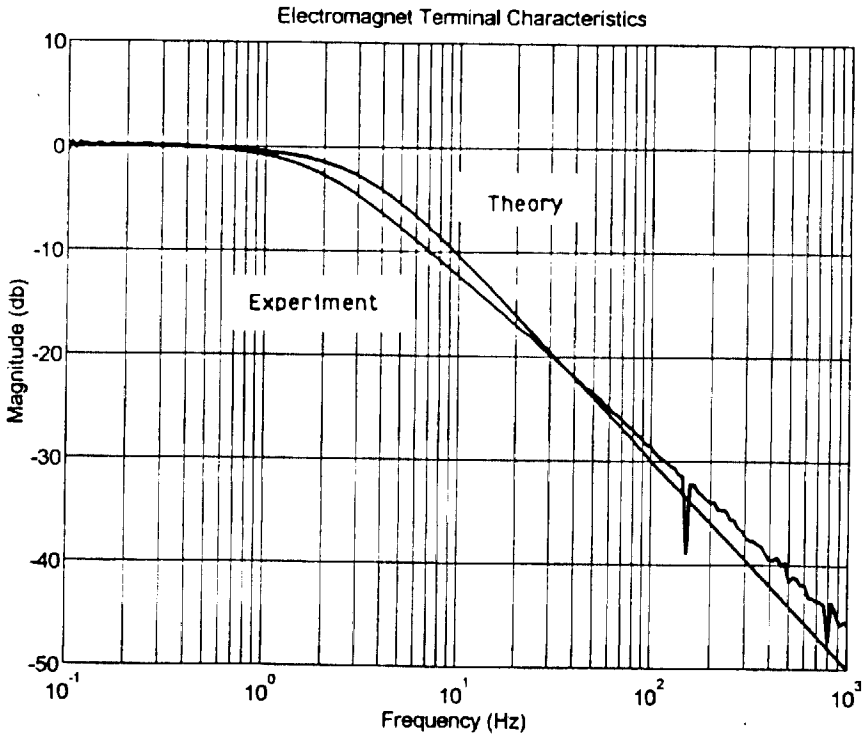

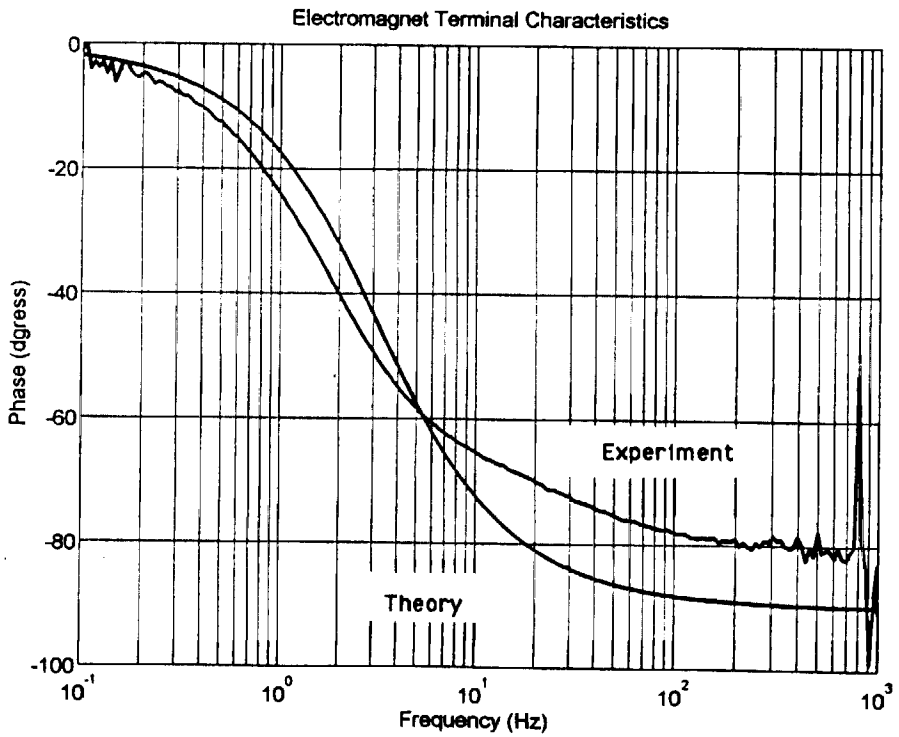

Figure 11 - Electromagnet Terminal Characteristics

APPENDIX

Matching Procedure for Eddy Circuit Parameters

If the governing equation is cast in the form :

$$B_Z = K_Z I \left(1 - \frac{A\, s}{1 + B\, s} \right)$$

- it is easily shown that the maximum phase shift will occur at a frequency :

$$\omega_{max} = \left(\frac{1}{(B(B\text{-}A))} \right)^{\frac{1}{2}}$$

- and that the maximum phase shift itself (a lag) will be :

$$\phi_{max} = \mathrm{Tan}^{-1} \left(\frac{A}{2\sqrt{(B(B\text{-}A))}} \right)$$

Once the experimental values of maximum phase shift and frequency for maximum phase shift are found, these expressions yield the modified estimates of the parameters A and B.